submitted to Composites Science & Technology
March 1997

AN IMAGE ANALYSIS TECHNIQUE FOR EVALUATING INTERNAL DAMAGE IN GRAPHITE/POLYIMIDE FABRIC COMPOSITES

K. Searles [1], J. McCarthy [2] and M. Kumosa [3]

[1,2] Materials Microanalysis Laboratories
Department of Materials Science and Engineering
Oregon Graduate Institute of Science and Technology
P.O. Box 91000, Portland, OR 97291-1000

[3] Center for Advanced Materials and Structures
Department of Engineering
University of Denver
2390 South York, Denver, CO 80208

Abstract

The purpose of this paper is to suggest a possible technique for evaluating internal damage in fabric composite materials. The technique presented in this work is based on capturing and performing a qualitative analysis of scanning electron microscope (SEM) images of damage from planar specimen slices and then reassembling the slices in three-dimensional space. This method has been applied to evaluate damage in graphite/PMR-15 fabric Iosipescu specimens tested in shear. Three-dimensional damage maps have been presented and the extent of damage through the thickness of a graphite/PMR-15 Iosipescu specimen has been determined. The same approach could be used for the evaluation of internal damage in other composite systems.

[1] Graduate Research Assistant
[2] Research Assistant Professor
[3] Research Professor, to whom correspondence should be addressed

1 INTRODUCTION

The present work is concerned with developing acceptable imaging techniques for determining the extent of in-plane and through-thickness damage in Iosipescu composite specimens tested under shear dominated, biaxial loading conditions. Although restricted to graphite/PMR-15 woven fabric composites in this paper, the imaging techniques could also be generalized to include other composite systems.

The Iosipescu test [1], originally intended for measuring elastic shear properties of isotropic metals, was subsequently extended by Walrath and Adams [2,3] to include composite materials. This method has evolved into one of the more popular tests for the shear characterization of composite materials due to simple loading configurations, specimen geometries and lower specimen preparation costs. The fixture used in this analysis (Figure 1a) is a modification based upon the traditional Iosipescu shear test [3] and the Arcan in-plane stress method [4]. It was designed by Broughton, Kumosa and Hull [5,6] with the capability to determine failure properties for a plethora of composite systems tested in pure shear and a biaxial combination of shear/tension or shear/compression (Figure 1b). The fixture consists of two stainless steel halves, each 100 mm wide. One half of the fixture displaces downward while the other is fixed. Four loading blocks, two on each side are symmetrically offset relative to the specimen centerline (notch-root axis) and generate uniform, biaxial, shear dominated stress fields at the specimen center. The loading blocks are fixed to disks which house the double edge-notched beam specimen (Figure 2) and are indexed according to relative angle of the applied load. Each index represents a 5° increment with the total maximum rotational range being ± 45° shear/tension (- or clockwise) or shear/compression (+ or counter-clockwise). The holes in the center of each rotating disk allow for strain gage attachment, acoustic emission waveguides and viewing during testing. Previous analyses have adopted the fixture for obtaining mixed mode failure properties unidirectional graphite/Epoxy, Ti/SiC composites and Teak wood [5-9].

2 POTENTIAL FAILURE MECHANISMS

Recently, the biaxial failure properties of quasi-isotropic graphite/polyimide, textile structural composite Iosipescu specimens were investigated using the biaxial Iosipescu method at room temperature [10,11]. The composite systems, fabricated at the NASA Lewis Research Center, met the following specifications:

Fabric:	T650-35, 8-Harness Satin Cloth
Ply Layup:	16-ply with floating undulations (warp-aligned)
Matrix:	PMR-15
Q and R:	Ultrasonic inspection

After testing several Iosipescu specimens in shear, shear/compression and shear/tension[10], it was noted that the failure process was significantly different in comparison to previously reported failure mechanisms observed in either isotropic materials or unidirectional composites [5-9]. Moreover, the mechanical response of the Iosipescu specimens appeared to be dependent on the external biaxial loading conditions.

2.1 Failure of Unidirectional Iosipescu Specimens

For 0° unidirectional specimens (fibers oriented along the long axis of the Iosipescu specimen), failure under all loading conditions, either shear or biaxial, occurs as a result of axial splits initiated at the roots of the notches [5-9]. These splits form parallel to the fibers and propagate on one side of the notch tip away from the nearest loading point. The split formation is always manifested by two successive drops on the load-displacement diagram. Unidirectional composite specimens with 90° fibers (fibers oriented along the notch root axis) always fail catastrophically. For all loading angles, cracks originate at the notch root and propagate in an unstable manner parallel to the fibers.

The failure process in both 0° and 90° oriented unidirectional Iosipescu specimens can be easily determined since the failure of the specimens is usually through the thickness and the cracks are visible on the specimen surface. For the fabric composites, the failure process is much more complex and can vary through the thickness. In this case, the failure characteristics cannot be determined by examining the specimen surface only, therefore a detailed analysis of damage through the specimen thickness is required.

It has also been reported [12] that cross-ply graphite/epoxy laminates tested in shear using the traditional Iosipescu method failed in a stable manner. The failure was associated with large damage zones developed in the gage sections of the specimens. It is feasible to assume, at this point, that failure characteristics of the graphite/PMR-15 woven fabric will resemble those observed in the cross-ply specimens subjected to shear.

2.2 Failure of Graphite/PMR-15 Fabric Iosipescu Specimens

The load/displacement diagrams for the graphite/PMR-15 Iosipescu specimens tested in shear as well as shear/tension and shear/compression are shown in Figure 3. The curves presented in Figure 3 exhibit a maximum load followed by a sudden drop. This phenomenon was observed for all specimens tested in this study. The results also reveal a general trend towards stability of the process after the initial "damage trigger" as compared to graphite/epoxy laminates. Specimens tested under shear/tension loading conditions were the only exceptions to those observations. Here, the tests resulted in a significant increase in load for very high displacements followed by another "trigger". In all cases, this process repeated itself two to three times.

The tested specimens were examined and the most important **surface** features of their damage zones were determined:

1. Large damage zones developed in the gage section of the specimens were observed. The zones consisted of multiple surface cracks (see Figure 4).

It was almost impossible to determine the mode of failure most prevalent i.e., intralaminar, interlaminar or translaminar.

2. The damage zones were associated with significant and permanent out-of-plane deformations (bulging) on the surfaces of the specimens (see Figure 5). It seems that the specimen surface bulging developed just before the "damage trigger".

3. The damage zone morphology was almost identical for all loading angles. It appears, however, that damage zone size was slightly smaller in those samples tested in shear/compression in comparison to the zones developed under biaxial shear/tension loading conditions.

2.3 A Need for Refined Image Analysis Techniques

In order to thoroughly evaluate the damage zone development and mode or modes of failure most prevalent in the graphite/PMR-15 Iosipescu specimens under shear dominated, biaxial loading conditions, we need to evaluate the damage not only on the specimen surface, but also within the specimen. This requires an acceptable method for specimen dissection and image reconstruction. Typical methods currently in use rely on SEM backscatter techniques, texture or "rug" mapping, stereo pairs, z-projections, mesh generation and solid modeling. The method proposed in this paper will combine several of those ideas and yield an outcome with potentially more useful information regarding the initiation and development of damage in the specimens through their thickness.

3 IMAGE ANALYSIS PROCEDURE

The experimental procedure followed in this investigation was to capture and perform a qualitative analysis of scanning electron microscope (SEM) images from planar specimen slices, reassemble the slices in 3-dimensional space and visualize the net volumetric effects of damage.

One graphite/PMR-15 Iosipescu specimen tested in shear was analyzed. The load/displacement diagram for this particular specimen is shown in Figure 3. The internal damage in the gage section of the shear tested specimen was investigated.

3.1 Specimen Preparation

Following mechanical testing, the central section of the 80mm x 20mm specimen was removed along the SEM cutting planes (see Figure 6) via a Buehler Isomet low speed saw. All cuts were made using a diamond tip circular blade and copious amounts of fluid. Once the central section was removed, the surface of the sample was saturated with Gatan G-60 quartz-crystalline epoxy under 45 psi of pressure. The epoxy has a fairly low viscosity, needs to be temperature cured and is capable of making sub-micron adhesive joints.

After 24 hours of pressurization and curing, the specimen was placed in a 2.5" diameter container and hard mounted with specimen preparation epoxy. This allowed for stable mounting in the SEM and safer handling during polishing with lapping disks. The encapsulated section necessitated the need for a special holder capable of indexing up an equidistant value after each slice removal in order to maintain the appropriate working distance in the SEM.

3.2 Image Capturing

The hard mount was initially polished until the top planar surface of the specimen section was exposed. This was designated as the z-axis reference surface and tagged index-00. Two sets of 3 locator holes were used to mark the regions of interest (ROI's). One of the hole sets was located at the section center and the other set was located at the top notch as shown in Figure 7. The holes served to define x-y planes by which sequential slices could be accurately aligned in the SEM.

After exposing index-00, the section was sputtered with approximately 150 Å of Au-Pd deposit from a Technics Hummer II D.C. Sputtering System. This was done to prevent localized charging and poor image sampling during the image capturing process. All images were captured using the Zeiss Model 960 analytical scanning electron microscope in backscatter mode. The working distance was fixed at 16mm, the beam current was 20kV and the maximum magnification set by the screen capture board and locator hole separation was 45X. Subsequent to capturing index-00, a 350μm ± 25μm slice was removed to expose the next layer (index-01) and each exposed layer was again saturated with epoxy. Capturing and polishing was consecutive through index-04. At this point, it was stopped because symmetry along the mid-line was assumed and ensuing indexes would mirror previous indexes.

The entire specimen preparation and image capturing processes were subsequently repeated using an untested sample in order to determine the effect of the specimen preparation process on the damage initiation in the composite.

3.3 Image Processing

Subsequent to capturing each index, two-dimensional damage maps were generated on a 120 Mhz Pentium PC using the public domain program NIH Image (developed at the U.S. National Institutes of Health and available on the Internet at http://rsb.info.nih.gov/nih-image/). Indexes 00-04 were treated separately for both the center target and the notch target. A low-pass smoothing filter was applied in conjunction with a 3x3 median (rank) filter to each index and threshold was manually adjusted. This established a perimeter outline for each area of detected damage, i.e., determined via contrast changes. For this analysis, 3x3 smoothing kernels of the form:

$$\begin{bmatrix} 1 & 1 & 1 \\ 1 & 1 & 1 \\ 1 & 1 & 1 \end{bmatrix} \quad \text{or} \quad \begin{bmatrix} 1 & 1 & 1 \\ 1 & 4 & 1 \\ 1 & 1 & 1 \end{bmatrix}$$

were assumed to remove noise from one-dimensional or two-dimensional signals while preserving image information content. According to Bovik, Huang and Munson [13], the two-dimensional median filter may be defined as follows:

$$\hat{X}_{i,j} = \text{median}\{X_{i',j'} : (i', j') \in W(i, j)\}$$

where W(i, j) reflects centering of the filter window at image coordinates (i, j). Essentially, each pixel within a 3x3 neighborhood was replaced with a median value or all 9 pixels were sorted and the center replaced with a median from the neighborhood. Application included median, multi-pass prefiltering to suppress noise, improve thresholding and yield a consistent estimation of edges.

Once edge detection was complete, the maps were stacked in order and averaged, resulting in two-dimensional composite skeletons for each target. At this point, a partial quantitative analysis was made regarding the location and significance of damage and each outline was tagged as an object, counted and analyzed to determine area fractions of damage as a function of depth from index-00 (section surface). All tagged objects were analyzed using the public domain program UTHSCSA Image Tool 1.25 (developed at the University of Texas Health Science Center at San Antonio, Texas and available from the Internet by anonymous FTP at maxrad6.uthscsa.edu). Important characteristics of interest were the number of objects per index, the area of each object in sq. pixels, the mean area size ($\bar{x}$) and standard deviation (σ).

The final step in image processing procedures involved creating three-dimensional projections from manipulated image stacks. Each index was re-sampled and one of two sharpening 3x3 spatial convolutions was implemented using the kernels below:

$$\begin{bmatrix} -1 & -1 & -1 \\ -1 & 9 & -1 \\ -1 & -1 & -1 \end{bmatrix} \quad \text{or} \quad \begin{bmatrix} -1 & -1 & -1 \\ -1 & 12 & -1 \\ -1 & -1 & -1 \end{bmatrix}$$

A stack averaging plug-in was used on each of the index windows for a given target, producing a new image which was a pixel-by-pixel average of all index windows input into the stack. Each stack was processed into a surface using 3D View 1.00 (a public domain package available via http://physics.usyd.edu.au//mathewa/, developed as an add-on to NIH Image, by I. Huxley at the Physical Optics Dept, School of Physics, University of Sydney). According to Huxley, the program uses the *autofocus* method, finding surface heights from maximum intensity points in each column of pixels. In this analysis, surfaces were rendered for comparison from center and notch targets for both untested and mechanically tested Iosipescu sections.

4 IMAGE ANALYSIS RESULTS AND DISCUSSION

Figures 8 and 9 present two-dimensional maps for the shear tested graphite/polyimide Iosipescu specimen. The damage maps represent damage generated at the specimen center (Figure 8) and an area very close to the notch root (Figure 9), respectively. Each map denotes an approximate area on the specimen of 9 mm^2. Below each pixel-by-pixel averaged composite map a profile plot is presented showing the relative pixel contrast intensities by average gray values as a function of image width. The profile plot illustrates where the majority of cracks is distributed across each map and gives an indication of the size of cracks compared to the width of the map. From these maps, the location of damage in the examined areas can be estimated. Moreover, the crack propagation directions can also be determined.

After the shear test, the examination of the specimen surface revealed that the fiber bundles were reoriented with respect to their initial orientations [10]. Before the test, the bundles were oriented along both the long axis of the specimen and the notch root axis. Due to the large shear stresses generated during the Iosipescu shear test, bundle rotation took place in the middle portion of the specimen with the final bundle orientation being approximately 45° with respect to the notch root axis.

It is quite possible that the diagonal perimeters shown on the map represent a combination of intralaminar failures at the fiber bundle-matrix interfaces and failure at weave (warp/fill) undulations or "crimps".

Very little cracking is evident in the longitudinal direction (direction parallel to the long axis of the specimen). Vertical cracks (damage zones) dictated by much larger areas seem to represent the interlaminar failure process between the layers. It is possible that one or several of the vertical cracks could be associated with the load-drops shown in Figure 3. It is assumed that the shearing process forces the bundles to rotate and fail at the undulations as progressive intralaminar damage develops.

Simultaneously, the ends of the specimen move toward the center and kinking occurs. At some critical point during the loading process, interlaminar cracks develop and propagate, allowing the specimen to bulge outward from the centerline as shown in Figure 5. If the fracture toughness of the interfaces between the layers is low, some of the interlaminar cracks can propagate catastrophically along the specimen causing the load drops.

Since it is possible that damage could be induced into the specimen during the specimen preparation process, an untested specimen was also subjected to the polishing and epoxy curing procedure. Figures 10 and 11 represent untested (virgin) specimen center and notch target maps derived using the same techniques as previously mentioned. The differences between tested and untested center target maps are obvious as are the differences between tested and untested notch maps. The darker areas located on the maps for the untested targets most likely represent undulation resin pockets or *in situ* manufacturing voids. No visible damage to the composite caused by the specimen preparation process can be observed in Figures 10 and 11.

An important observation can be made by comparing the damage maps presented in Figures 8 and 9.

It is obvious that the amount of damage generated in the specimen center is significantly higher in comparison with the area close to the notch root. Therefore, it can be concluded that the specimen developed large shear stresses at its center without any stress concentrations present at the roots of the notches. This effect will most likely be observed in the specimens tested under the biaxial shear/tension and shear/compression loading conditions.

Damage area fractions represent the ratio of crack-inclusive areas to the total area. In this study, all images captured retained a 230,400 sq. pixel area or 480 x 480 resolution. Figure 12 illustrates the difference between the center and notch target measured damage as a function of depth from the surface. Clearly, damage accumulated near the Iosipescu specimen upper notch is less significant compared to the center. Also, the notch target area fraction oscillates between 3-4%, while the center target area fraction progresses from 8-12.5%. It appears that the shear initiated, catastrophic failure (the load drop in Figure 3) may originate near the specimen centerline and propagate outwards through the thickness and the specimen length. Figure 13 compares respective targets in the untested material, showing ranges from 0.3-0.68%. These results seem reasonable and tend to enforce the belief that polishing does not significantly alter the state of the material after testing.

Figures 14a and 14b show the projected three-dimensional reconstruction of the center and notch SEM targets from an assembly of index pairs 00-04. It can be seen from these figures that damage near the notch is not as pronounced and the majority of cracks follow diagonals similar to patterns where the warp/fill undulations are located. The projections give the illusion of transparency, but they actually represent a compilation of depth and intensity maps derived from the two-dimensional crack-laden stack averages. The darker corner areas are portions of the holes used to align each image from surface to sub-surface in sequence.

Finally, figures 15a and 15b show 3-D projections of untested material assembled in the same manner as previously described. It should be noted that the regularly shaped flaws are indicative of resin rich pockets, voids or imaging aberrations and show no propensity towards the initiation of crack sites during the specimen preparation process.

5 CONCLUSIONS

The following conclusions can be drawn from the results presented in this study:

1. The proposed image analysis technique can be successfully applied to investigate damage initiation and development in woven textile composites. Three-dimensional damage maps for a shear tested Iosipescu woven textile composite specimen have been generated. It has been shown that the specimen preparation process does not alter the state of damage intact after testing.

2. It appears that for 8-harness woven textile composites such as graphite/PMR-15, the presence of relatively sharp notches in the Iosipescu specimens does not affect the failure process. It has been found that the majority (50% more) of damage occurs in the central area of the specimen gage section. No significant damage has been detected at the roots of the notches. Therefore, it can be concluded that for this particular composite system, the Iosipescu shear test provides a uniform stress field in the gage section of the specimen.

3. From damage area fraction results, the number and size of internal cracks have been determined through the specimen thickness. The amount of damage increases as a function of the sub-surface depth and it is believed that this behavior is parabolic in nature with the maximum amount of damage occurring in the vicinity of the specimen mid-line. This seems to fit the explanation for the symmetrical out-of-plane deformation or bulging on the front and back side of the specimen.

ACKNOWLEDGEMENTS

This work was supported by the Air Force Office of Scientific Research and the National Science Foundation under research grants F49620-96-1-0314 and CMS-9696160, respectively. The authors wish to thank Mr. Mike Castelli of the NASA Lewis Research Center for his strong technical support and materials.

REFERENCES

1. N. Iosipescu (1967), "New Accurate Procedure for Single Shear Testing of Metals," *Journal of Materials 2*(1): 537-566.

2. Walrath, D. E., and D. F. Adams (1983), "The Iosipescu Shear Test as Applied to Composite Materials," *Experimental Mechanics 23*(1): 105-110.

3. Adams, D. F., and D. E. Walrath (1987), "Further Development of the Iosipescu Shear Test Method," *Experimental Mechanics 27*(2): 113-119.

4. Arcan, M., and Hashin (1978), "A Method to Produce Plane-Stress States with Applications to Fiber Reinforced Materials," *Experimental Mechanics 13*(3): 141-146.

5. Broughton, W. R., Kumosa, M. and D. Hull (1990), "Analysis of the Iosipescu Shear Test as Applied to Unidirectional Carbon Fiber Reinforced Composites," *Composites Science and Technology 38*: 299-325.

6. W. R. Broughton (1989), "Shear Properties of Unidirectional Carbon Fiber Composites," Ph. D. thesis. Cambridge, U. K.: University of Cambridge.

7. Bansal, A. and M. Kumosa (1995), "Experimental and Analytical Studies of Failure Modes in Iosipescu Specimens Under Biaxial Loadings," *Journal of Composite Materials 29*(3): 334-358.

8. Balakrishnan, M. V., Bansal, A. and M. Kumosa (1997), "Biaxial Testing of Unidirectional Carbon/Epoxy Composites Using the Biaxial Iosipescu Test Fixture," *Journal of Composite Materials 31*(5): 486-508.

9. M. V. Balakrishnan (1995), "Application of the Biaxial Iosipescu Test Fixture for the Mechanical Characterization of Unidirectional Composites," M.S. Thesis. Portland, OR: Oregon Graduate Institute of Science and Technology.

10. Kumosa, M., Searles, K. and V. Thirumalai (1995), *Biaxial Failure Analysis of Graphite Reinforced Polyimide Composites.* Annual Progress Report to the Air Force Office of Scientific Research. Department of Materials Science and Engineering. Oregon Graduate Institute of Science and Technology. pgs 1-80.

11. Kumosa, M., Searles, K. and G. Odegard (April 30, 1997), *Biaxial Failure Analysis of Graphite Reinforced Polyimide Composites*, in the Proc. HITEMP, in press.

12. K. Hollman (1990), *In-Plane Shear Failure Analysis of Notched Composites.* Department of Aeronautical Structures and Materials. The Royal Institute of Technology, Stockholm. pgs 1-39.

13. Bovik, A., Huang, T. and D. Munson, Jr. (1987), "The Effect of Median Filtering on Edge Estimation and Detection", *IEEE Transactions on Pattern Analysis and Machine Intelligence 9*(2): 181-193.

LIST OF FIGURES

11. Two-dimensional map and corresponding profile plot of untested material notch target

12. Approximated area fraction as a function of depth from the specimen surface for both damaged material targets

13. Approximated area fraction as a function of depth from the specimen surface for both untested material targets

14. Reconstructed three-dimensional projections of damaged material targets created from intensity and depth maps a) center target, b) notch target

15. Reconstructed three-dimensional projections of untested material targets created from intensity and depth maps a) center target, b) notch target

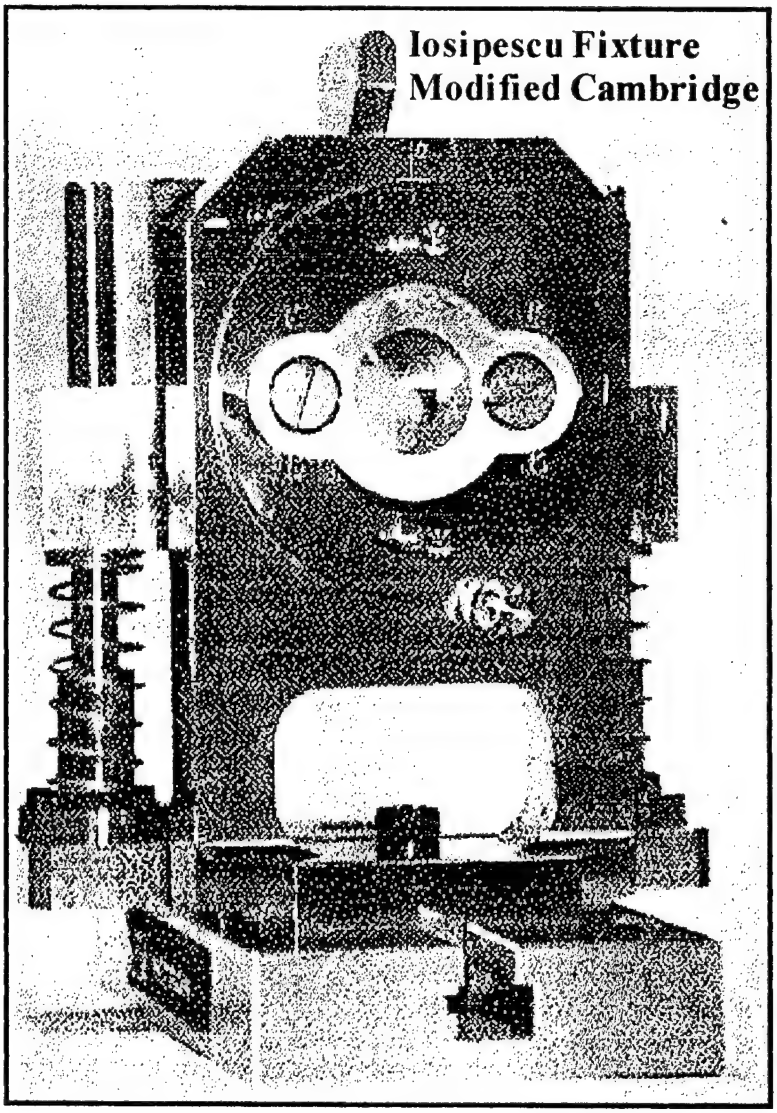

Figure 1a

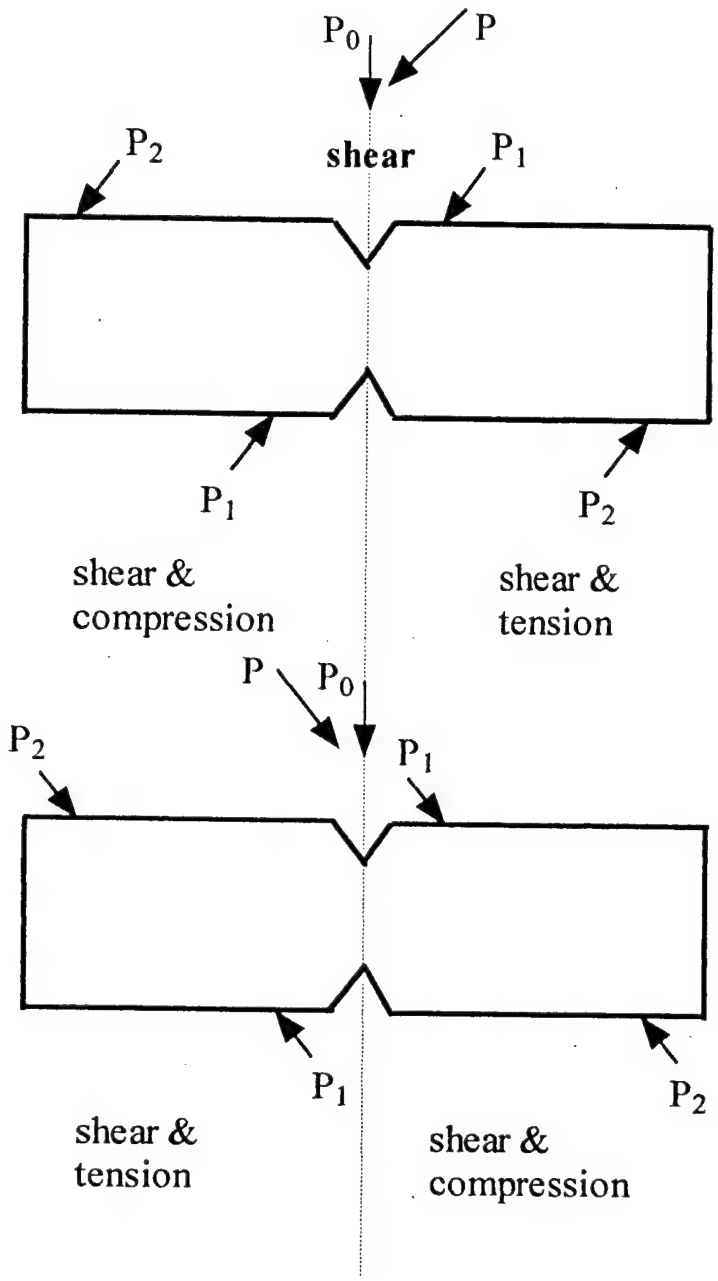
P0
P
P2
shear
P1
P1
P2
shear &
compression
shear &
tension
P
P0
P2
P1
P1
P2
shear &
tension
shear &
compression

Figure 1b

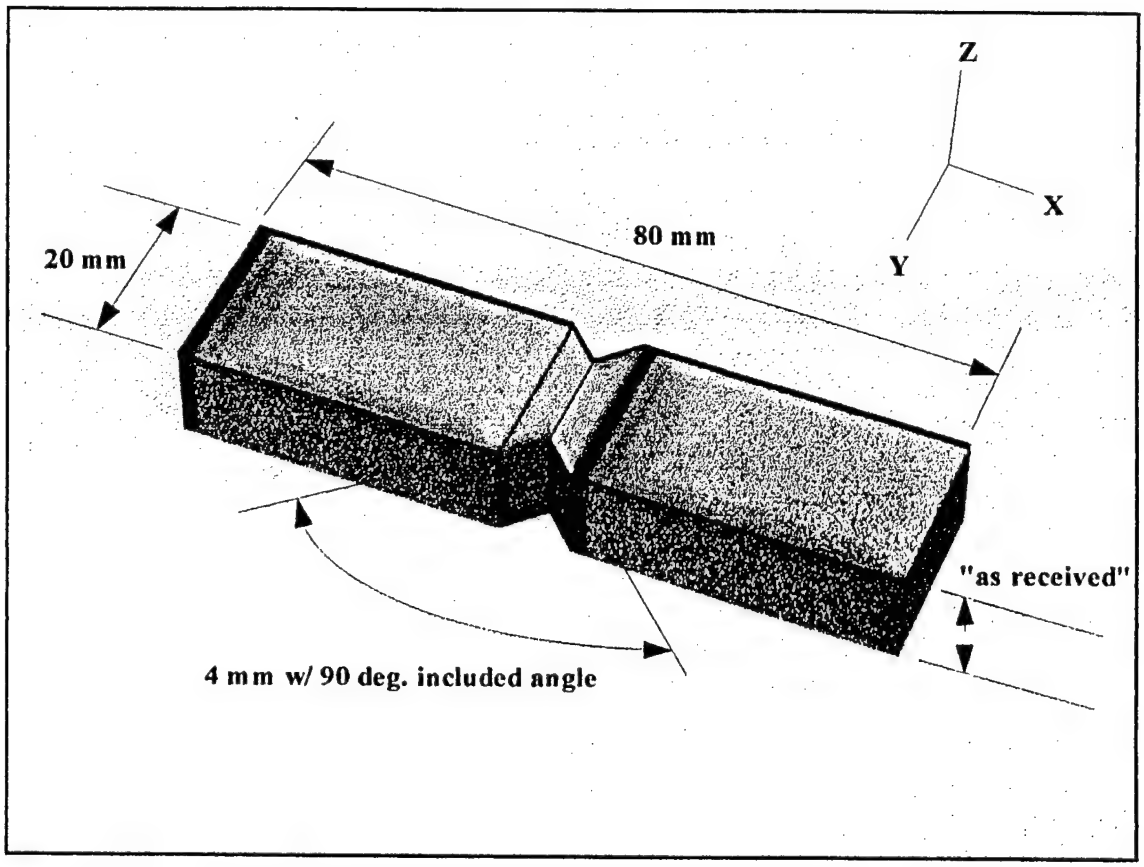

Figure 2

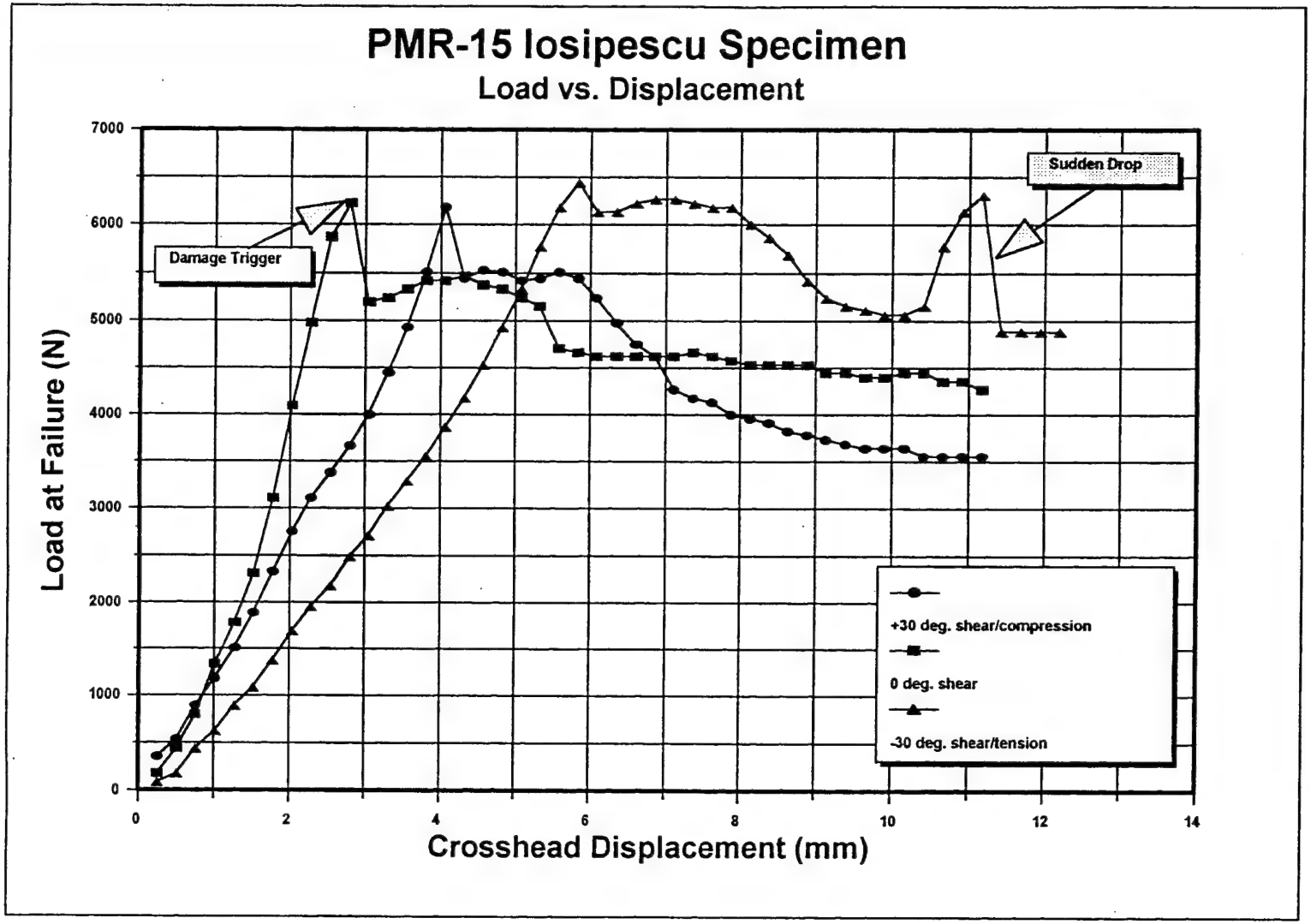
PMR-15 Iosipescu Specimen
Load vs. Displacement
Load at Failure (N)
Crosshead Displacement (mm)
Damage Trigger
Sudden Drop
+30 deg. shear/compression
0 deg. shear
-30 deg. shear/tension
0
1000
2000
3000
4000
5000
6000
7000
0
2
4
6
8
10
12
14

Figure 3

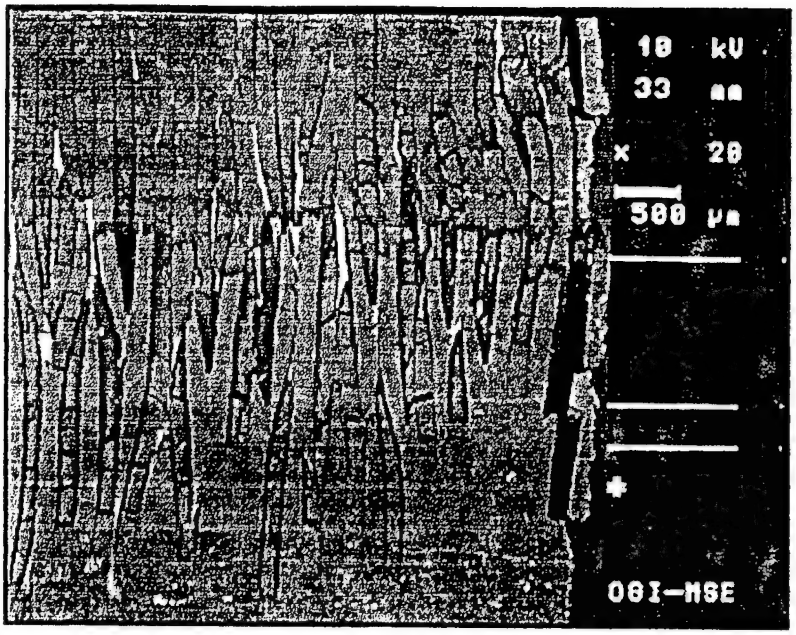

Figure 4

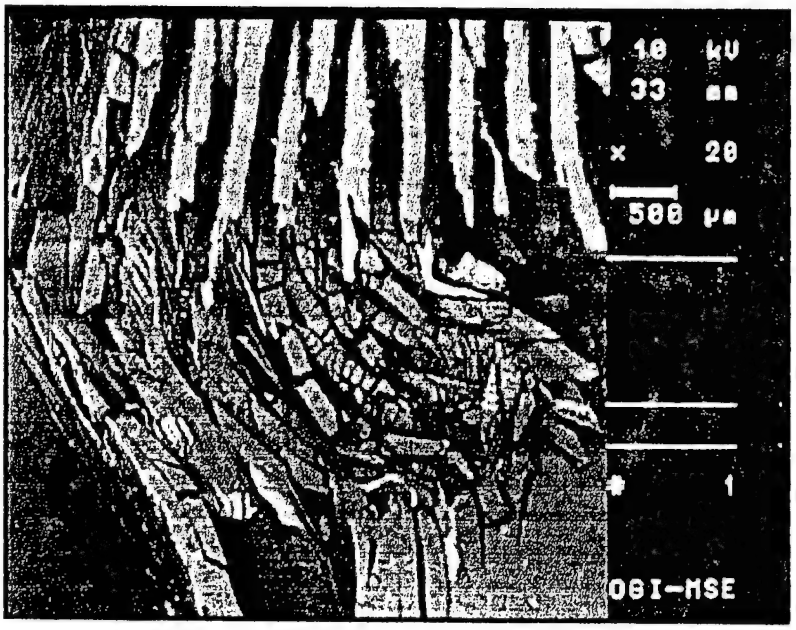

Figure 5

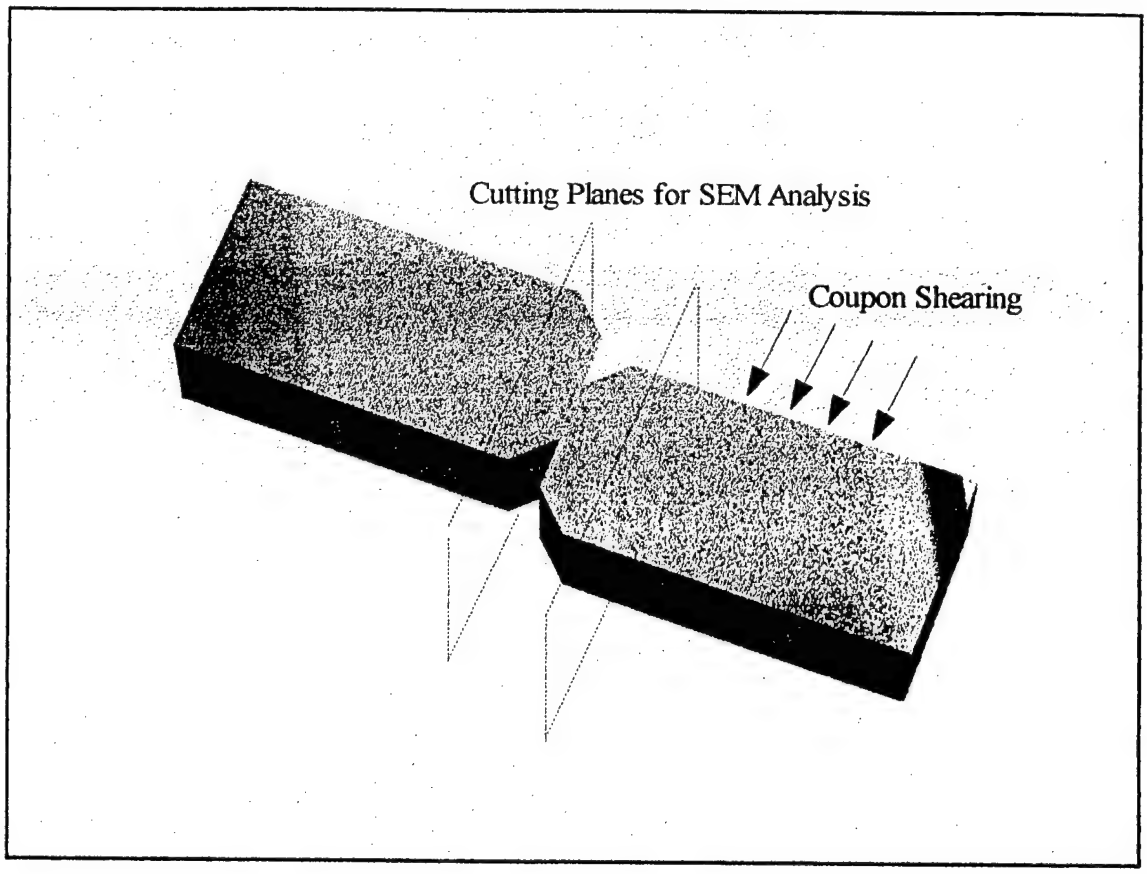

Figure 6

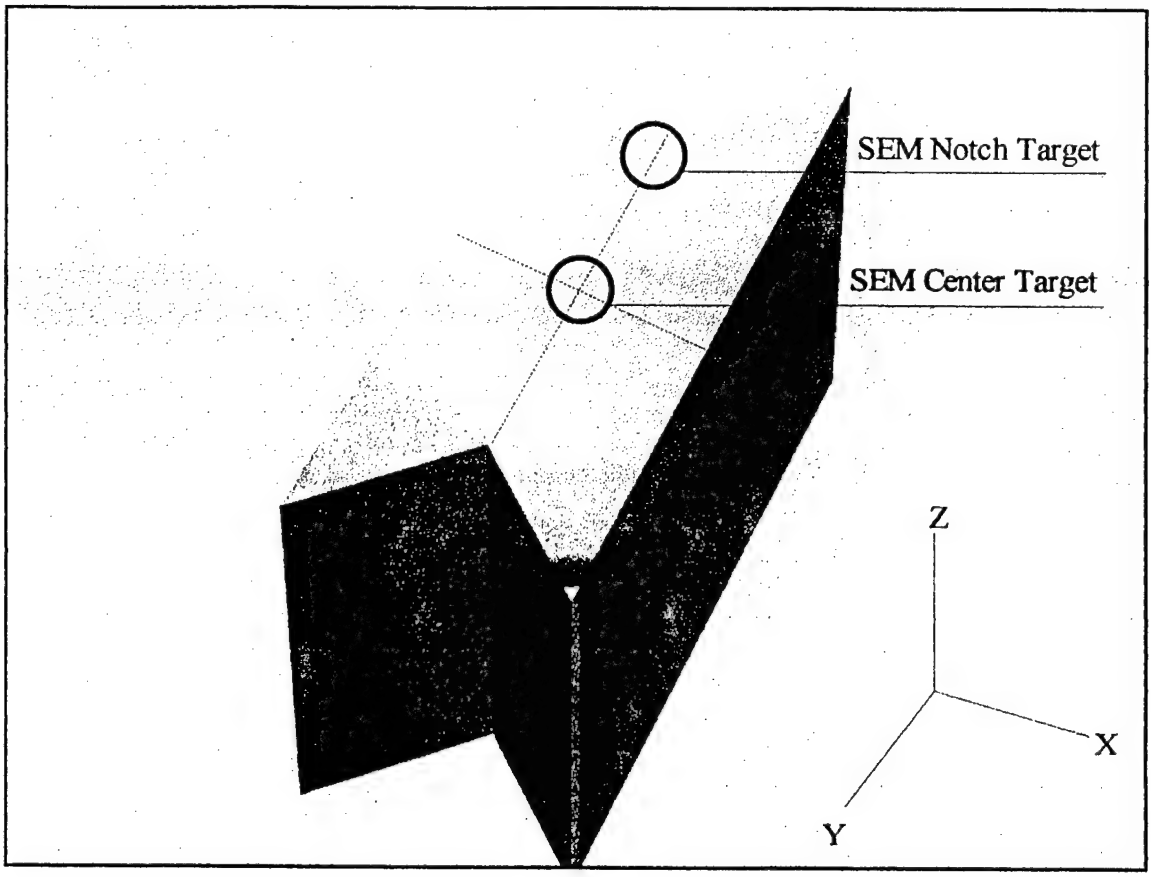

Figure 7

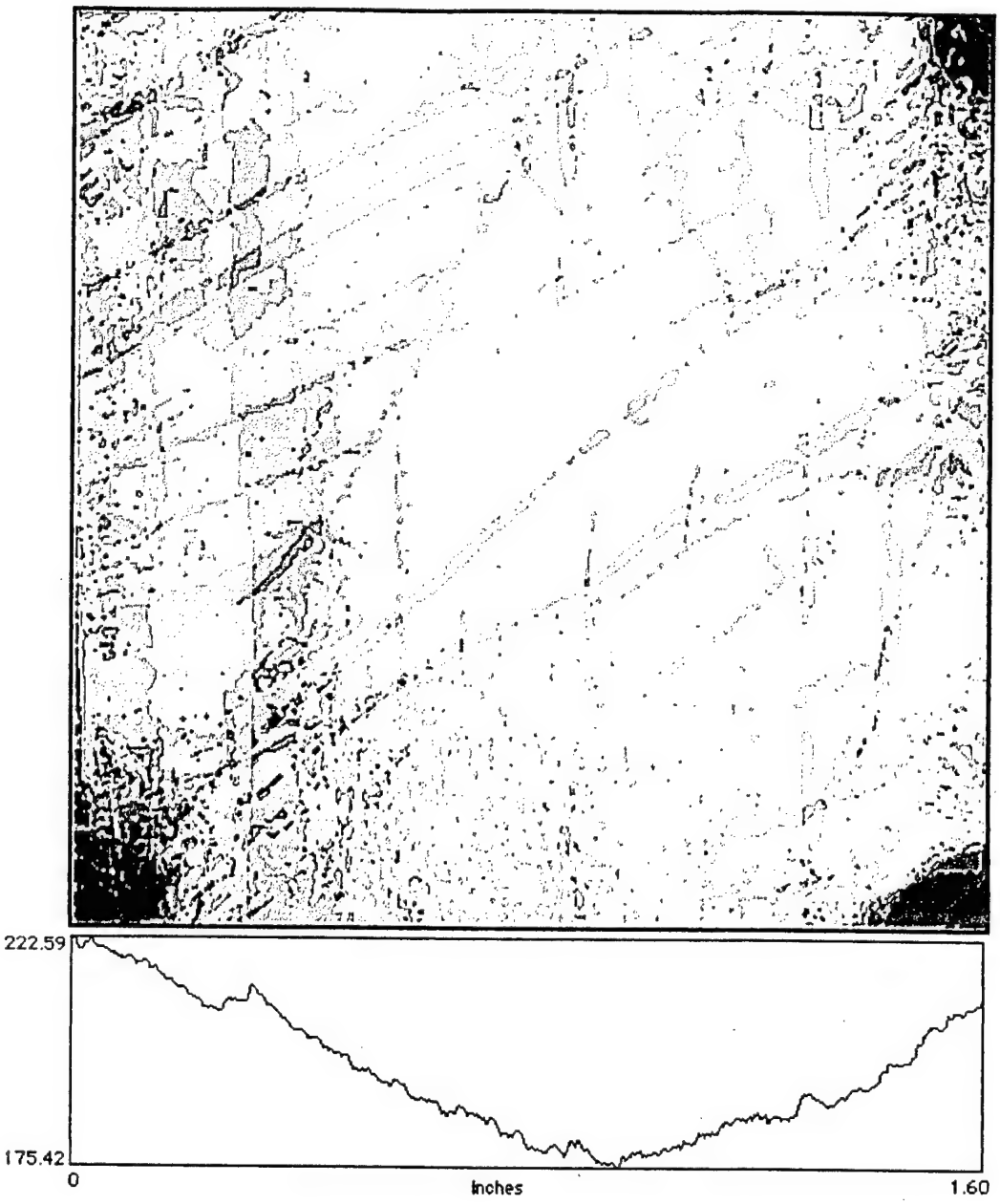

Figure 8

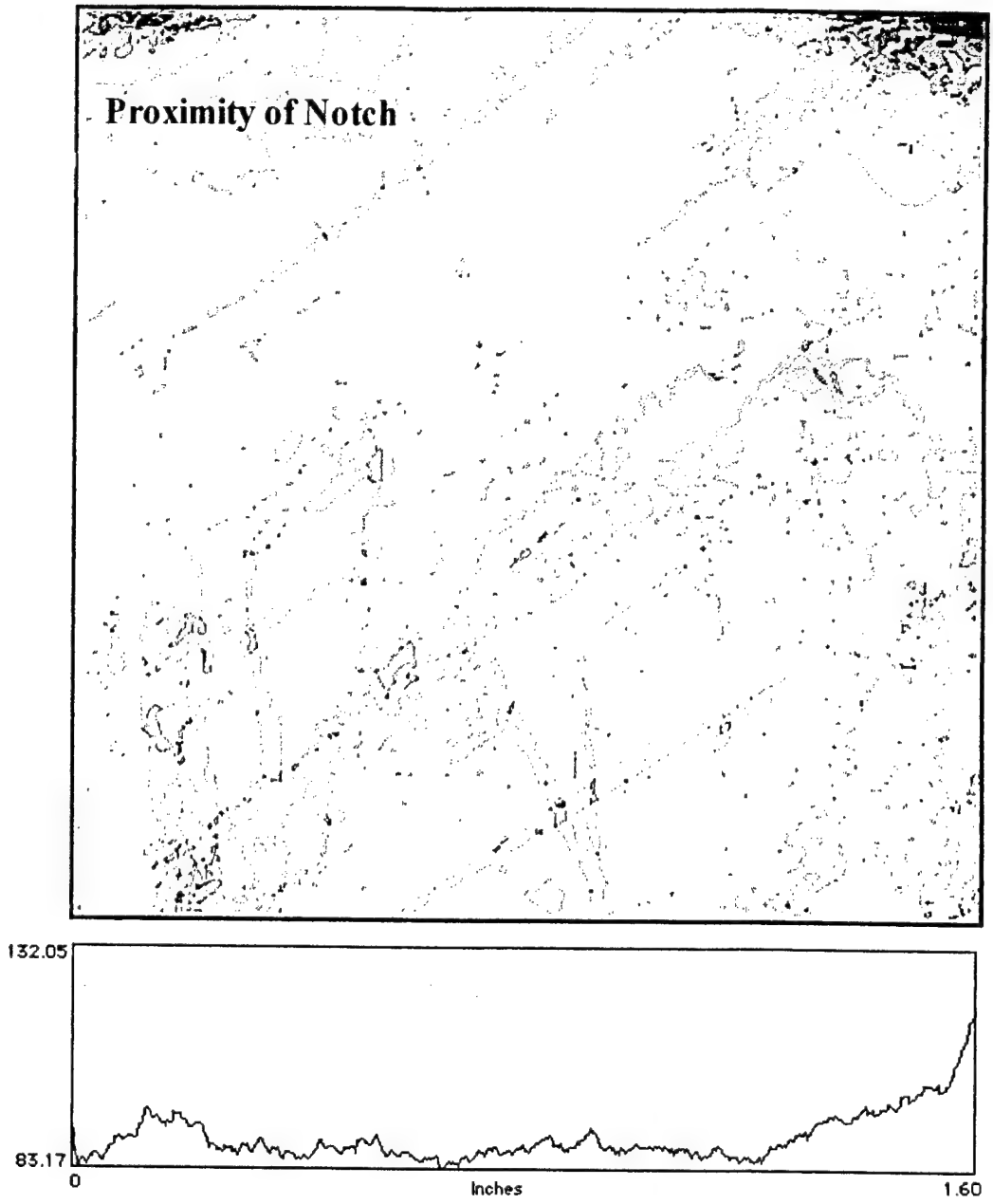

Figure 9

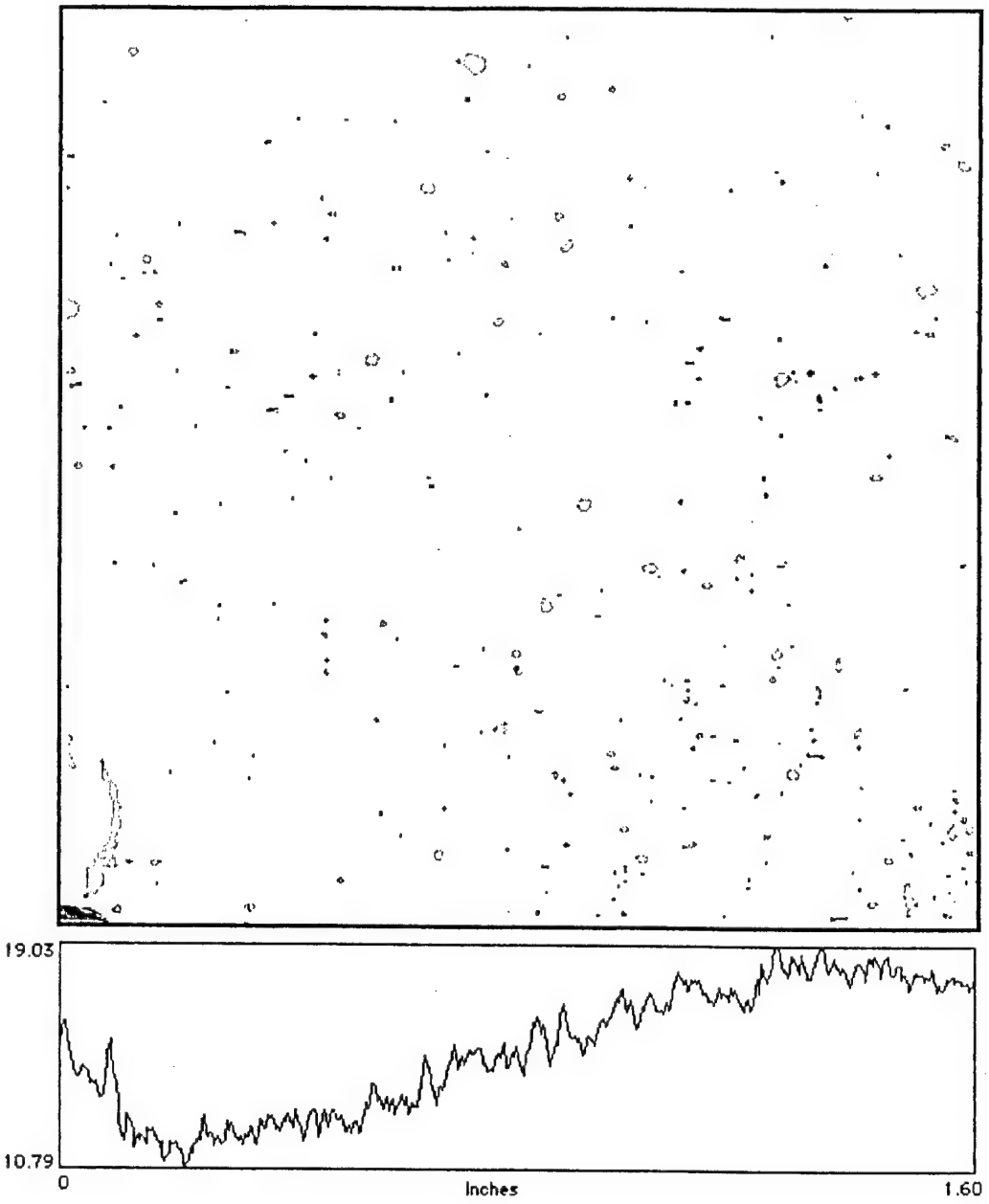

Figure 10

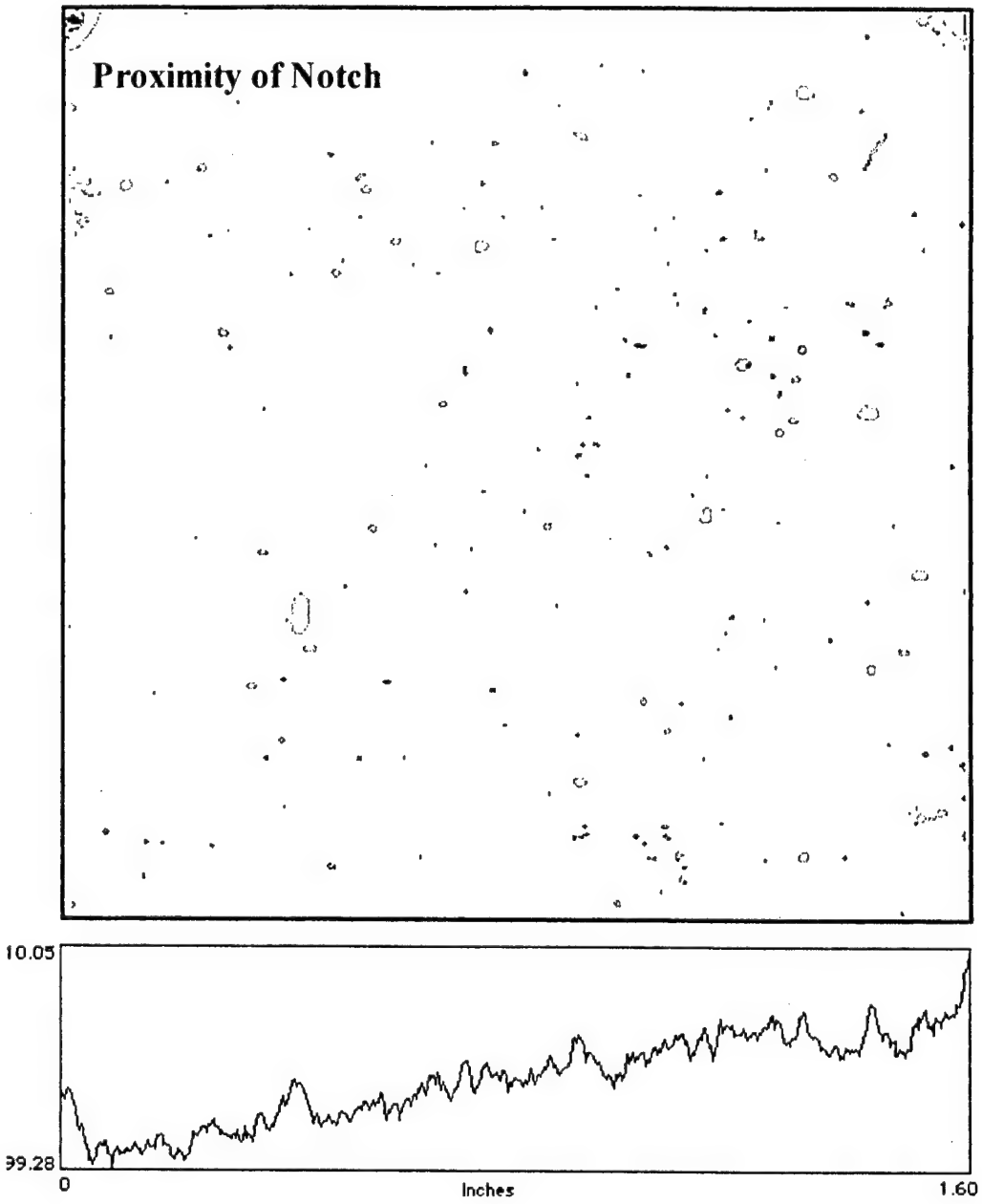

Figure 11

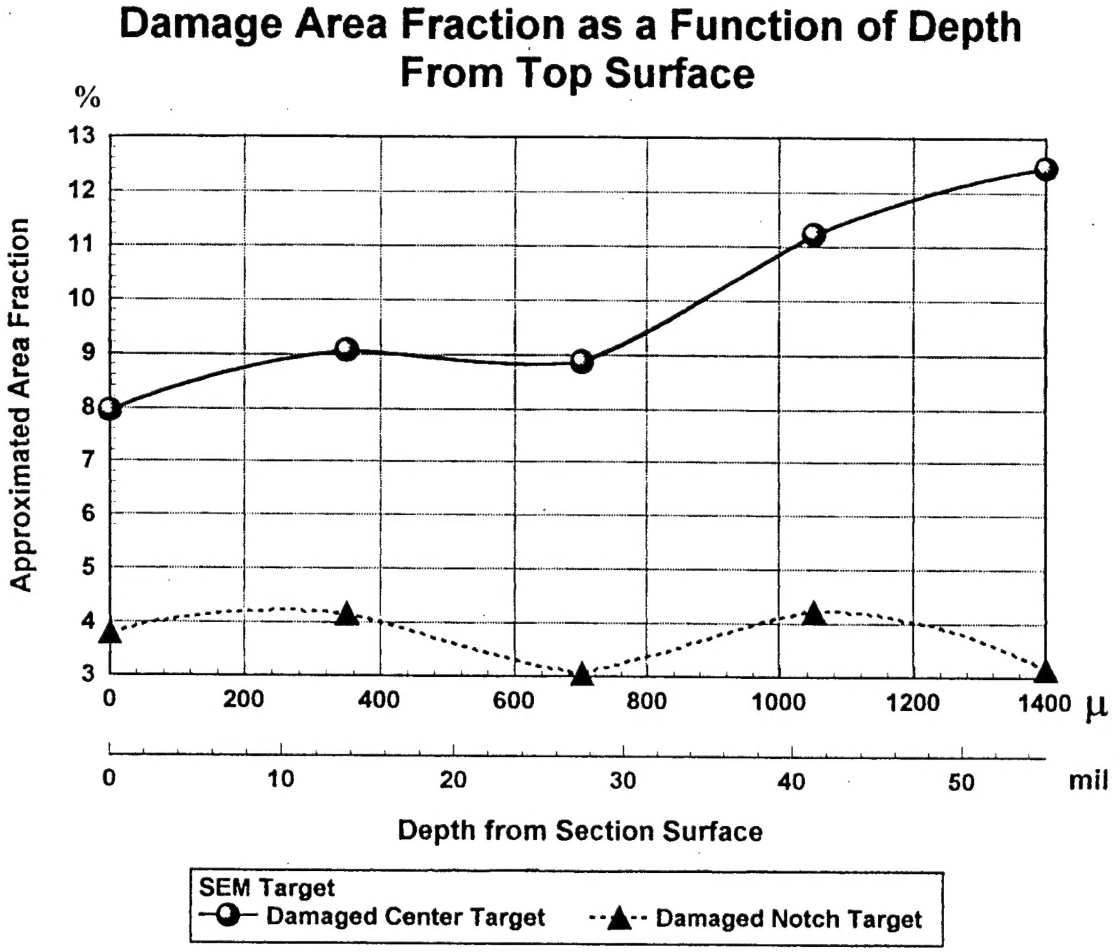
Damage Area Fraction as a Function of Depth From Top Surface
%
13
12
11
10
9
8
7
6
5
4
3
Approximated Area Fraction
0
200
400
600
800
1000
1200
1400
μ
0
10
20
30
40
50
mil
Depth from Section Surface
SEM Target
Damaged Center Target
Damaged Notch Target

Figure 12

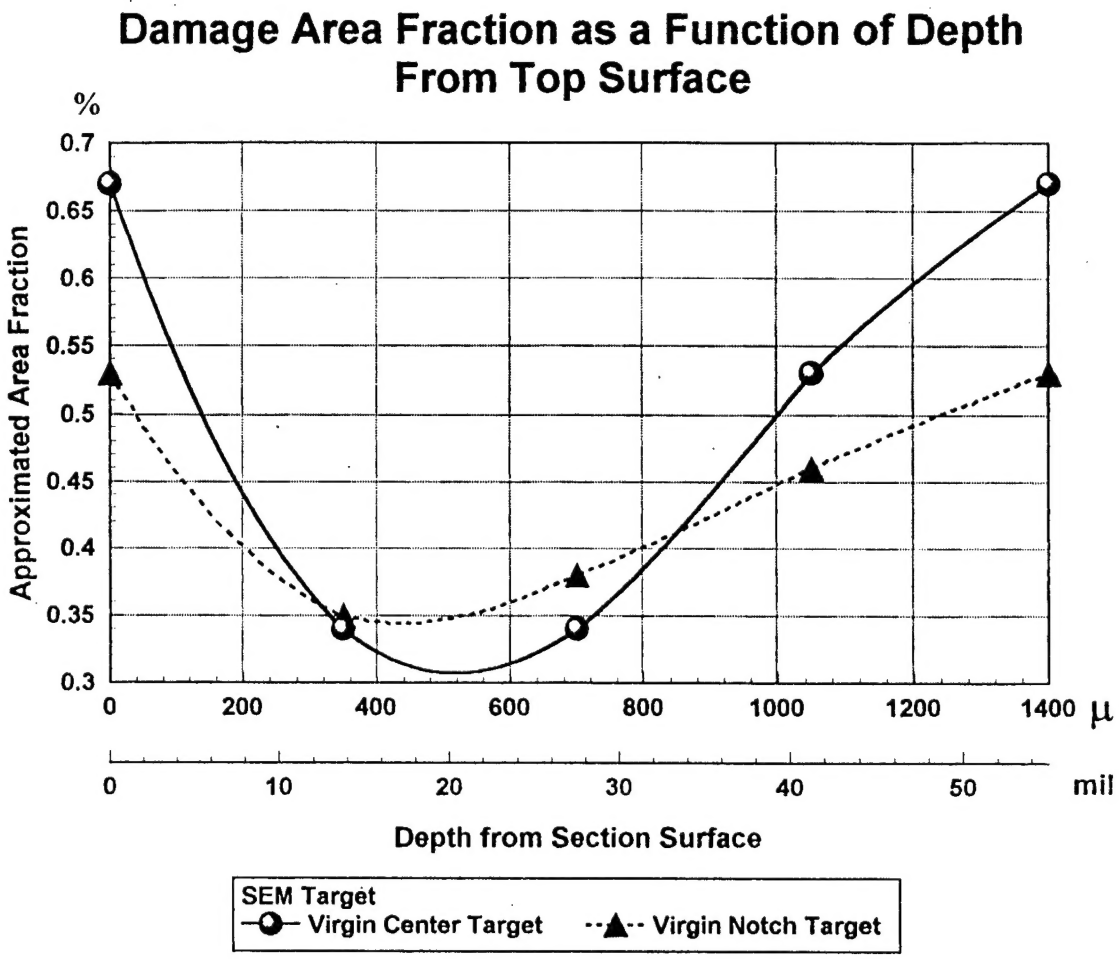
Damage Area Fraction as a Function of Depth From Top Surface
%
0.7
0.65
0.6
0.55
0.5
0.45
0.4
0.35
0.3
Approximated Area Fraction
0
200
400
600
800
1000
1200
1400
μ
0
10
20
30
40
50
mil
Depth from Section Surface
SEM Target
Virgin Center Target
Virgin Notch Target

Figure 13

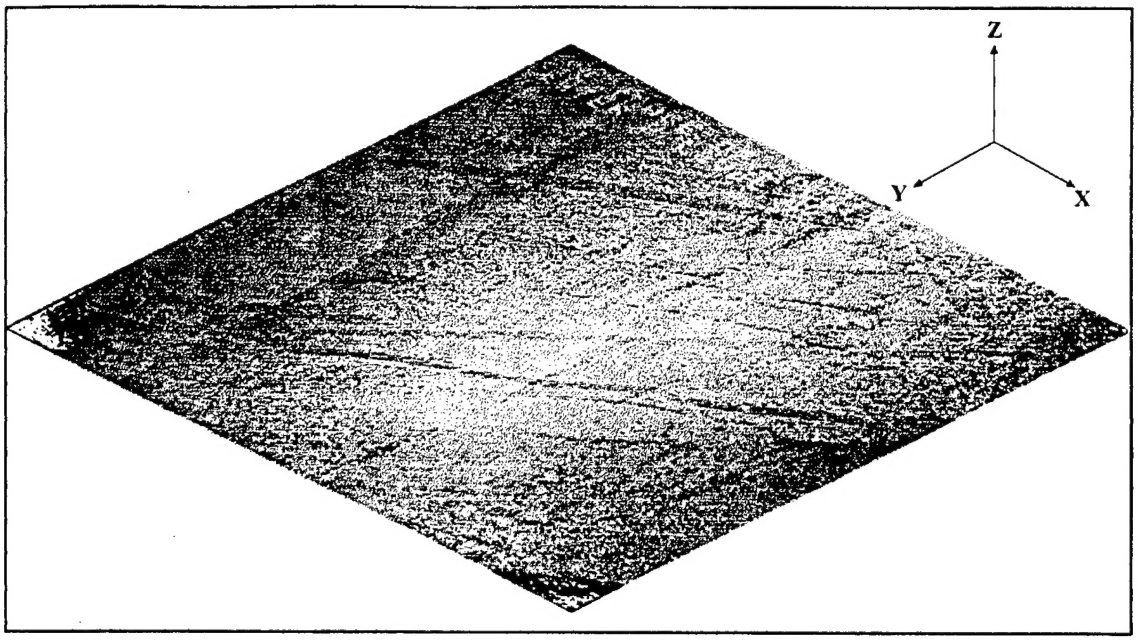

Figure 14a

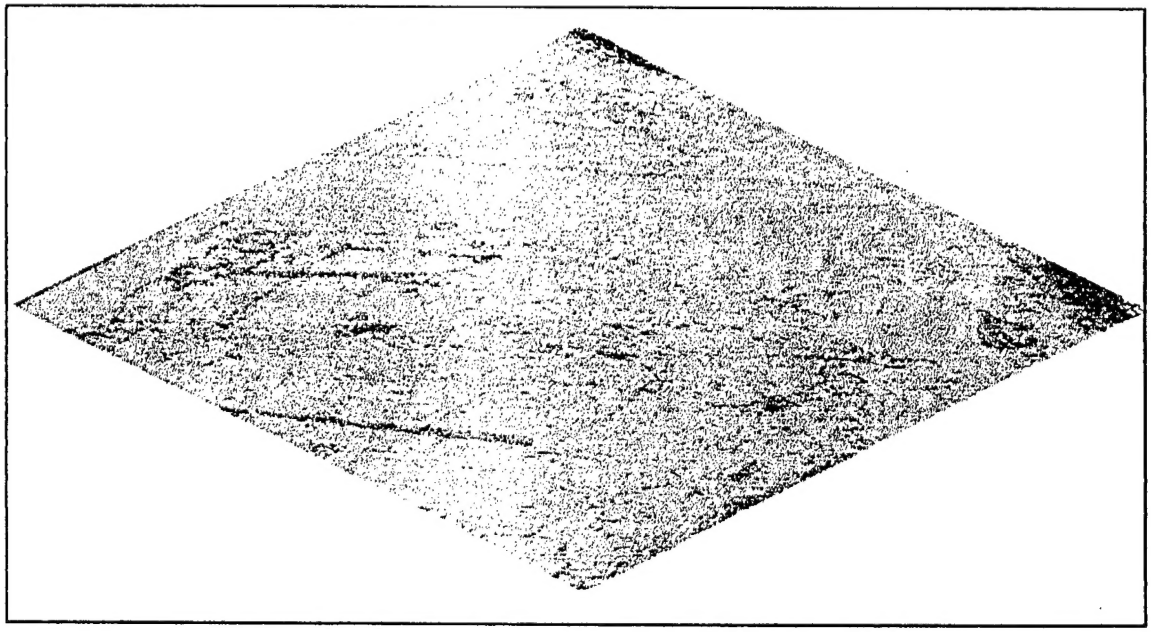

Figure 14b

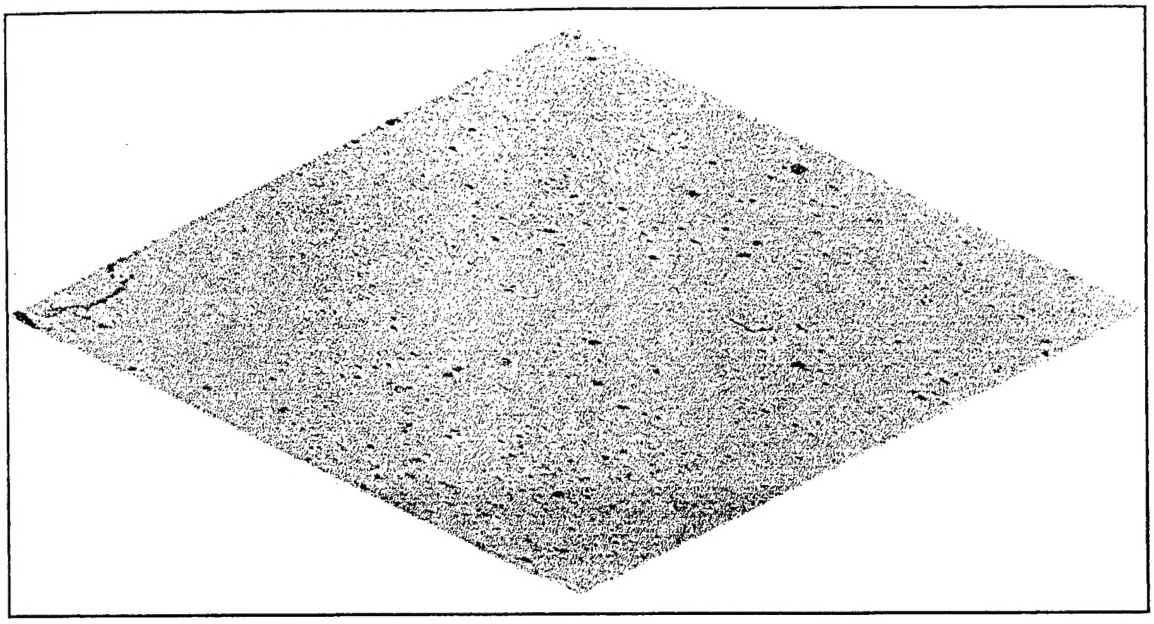

Figure 15a

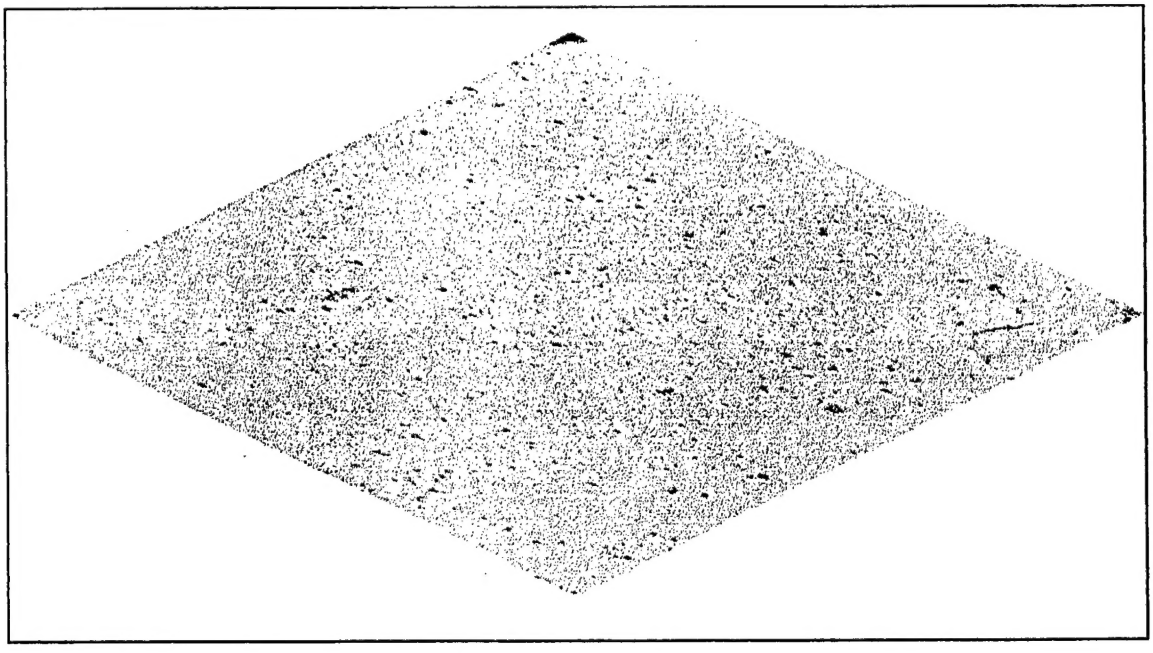

Figure 15b